

Influence of the Alumina Interface layer in Silica@Layered Double Hydroxide Core–Shell Particles

Philip Kenyon, Samuel Roberts, Zoë R. Turner, Nicholas H. Rees, and Dermot O'Hare*

Cite This: *J. Phys. Chem. C* 2024, 128, 12249–12258

Read Online

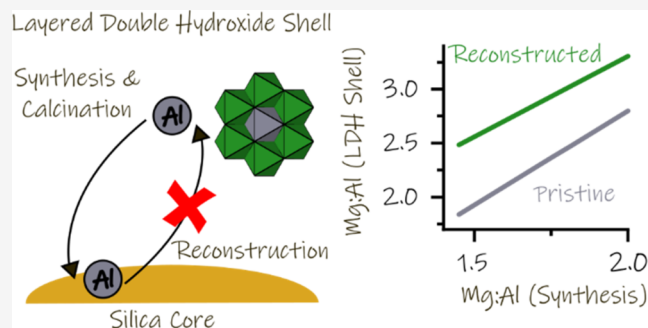
ACCESS |

Metrics & More

Article Recommendations

Supporting Information

ABSTRACT: We have studied the nature of the silica-layered double hydroxide (LDH) interface in silica@aluminum layered double hydroxide (silica@LDH) core–shell systems. This interface affects the composition of the LDH outer layer and the behavior upon calcination. By combining powder X-ray diffraction (XRD), thermal gravimetric analysis (TGA) and solid state magic-angle spinning nuclear magnetic resonance spectroscopy (ssMAS-NMR) we have demonstrated that the silica-LDH interface consists primarily of alumina. This interface is shown to require a consistent amount of aluminum which is removed from the outer LDH shell. By increasing the amount of aluminum used in the synthesis, Al-containing LDHs of desired M^{2+}/Al^{3+} composition can be formed. However, upon calcination the composition further changes due to the irreversible migration of aluminum ions from the LDH platelets into the interface. This is in stark contrast to the reversible transitions observed when LDHs are calcined to their layered double oxides (LDOs) and then reconstructed back to LDHs.



INTRODUCTION

Layered double hydroxides (LDHs) are a highly tunable class of two-dimensional (2D) inorganic materials with the general formula $[M_{(1-x)}M'_x(OH)_2]^{a+} [A_{a/n}^{n-}]_n \cdot mH_2O$ (hereafter designated MM' -LDH), where M and M' are most commonly divalent and trivalent cations, A^{n-} is an anion. For Mg_xAl -based LDHs pure crystalline phases are found when $0.33 \geq x \geq 0.18$.¹ These metal hydroxides form positively charged brucite-like layers, with the intercalated anions providing charge balance. As a range of divalent cations (including, but not limited to, Mg, Ca, Mn, Fe, Co, Ni and Zn) and trivalent cations (Sc, V, Cr, Fe, Ga and Al) can be incorporated in binary or higher mixtures it is possible to tailor these materials to a wide range of applications.² LDHs have been used as sorbents,³ supercapacitors,⁴ and particularly in catalysis,⁵ including acid–base catalysis,^{6,7} electrocatalysis^{8–10} and photocatalysis.^{11–15} However, agglomeration of the LDH platelets leads to a low surface area dense agglomerates which limits their use in a number of applications. There are a number of methods for increasing the LDH surface area including exfoliation and partial exfoliation by post-synthesis solvent treatments.^{16,17} While capable of greatly increasing the surface area, the residues of these solvents influence the chemical properties of these surfaces even after calcination,¹⁸ which will, in turn, influence the catalytic ability of these materials. An alternative approach is to template the LDH to a core material such as silica. The LDH platelets typically orient perpendicular to the surface, preventing agglomeration and leading to core–

shell material (silica@LDH),^{19,20} with surface areas over a magnitude higher than conventional LDH.¹⁹

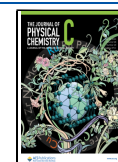
Silica@LDH core–shell structures have been synthesized and applied as catalysts,^{21–24} supercapacitors^{25,26} and sorbents for polluted water;^{27–29} both as core–shell structures^{21–23,27–29} and as templates for hollow-shell structures.^{24–26} Various forms of silica have been used to produce silica@LDH,^{19,30} and it has been demonstrated that by controlling synthesis conditions the density and orientation of the LDH platelets on the silica surface can be controlled^{20,23,31} and that it is also possible to partially exfoliate the platelets after the initial synthesis.³² While morphological control has been well demonstrated, there has been less focus on the LDH platelets in terms of composition. It has been demonstrated that magnesium–aluminum LDH forms covalent bonds between aluminum (Si–O–Al)^{19,20,24} and possibly magnesium (Mg–O–Al)^{21,22} and the silica core. This interface is observed to remain even when the silica core dissolves¹⁹ and could consume a significant portion of the aluminum (or magnesium) ions which would otherwise be incorporated into the LDH platelets in the outer layer.

Received: May 7, 2024

Revised: July 3, 2024

Accepted: July 3, 2024

Published: July 16, 2024



Understanding the nature of this interface is therefore essential to understanding the influence it will have on the chemical composition and subsequent reactivity of the LDH.

Pristine LDHs are used in many applications. However, calcination of the LDH is necessary for a number of catalytic³³ and environmental^{34–36} applications and also in the synthesis of certain LDHs via the memory effect, particularly for the incorporation of unusual anions.³⁷ For core–shell materials such as silica@LDH, it is therefore necessary to understand how the calcination process affects the two phases of the core–shell material. During the calcination of LDH, following dehydration, the layered structure collapses while the individual layers undergo dehydroxylation to form amorphous mixed metal oxides sometimes termed layered double oxides (LDO);^{38–41} it can be observed that there is significant migration of Al^{3+} from octahedral to tetrahedral interlayer sites, even at low temperatures ($<200\text{ }^{\circ}\text{C}$).^{38,39,41,42} LDO formation is often considered to be reversible upon rehydration, and the reformation of a layered LDH structure is easily observed by X-ray diffraction (XRD).⁴³ However, the extent to which this reconstruction takes place is debated,⁴⁴ for example it has been shown using ^{27}Al DPMAS NMR spectroscopy that after calcination and reconstruction not all tetrahedral aluminum is recovered,^{45–47} even at the low calcination temperature of $150\text{ }^{\circ}\text{C}$.⁴⁵ In contrast, complete reconstruction has been observed for some samples rehydrated after calcination to 450 or $550\text{ }^{\circ}\text{C}$.^{42,48} XAFS suggests changes in aluminum coordination environment at $150\text{ }^{\circ}\text{C}$ reverse upon cooling, and that LDH samples calcined at $450\text{ }^{\circ}\text{C}$ are identical to the directly synthesized LDH after rehydration using a stream of water vapor.⁴⁹ Despite this, spinel formation has been observed after repeated calcination at $400\text{ }^{\circ}\text{C}$ and rehydrating in aqueous solutions.⁵⁰ These conflicting results are likely due to the fact that reconstruction is dependent on the physical and chemical nature of the LDH and the method of rehydration.^{34,46,48,51–54} As the degree and reversibility of this migration may be different for core–shell materials and will influence the chemical composition of the LDH layers, it is important to understand how the migration of aluminum ions in Al-containing LDH changes in the presence of an interface with another material.

Currently, it is assumed that the chemical composition of the LDH shell in core@LDH hybrid materials reflects the ratio of the materials used in the synthesis, and it is not known if this changes significantly upon calcination or reconstruction. We propose to use, silica@LDH, which is a well established core–shell structure, with a known interface and many applications as a model compound, to determine (and where possible quantify) the influence of the core on the LDH shell, during synthesis and upon calcination and reconstruction. By understanding how the presence of a core (or an interface) influences the composition of LDH platelets, it can be better understood how to rationally design silica@LDH, and core@LDH materials more generally, with shell compositions specifically engineered for catalysis and materials applications.

METHODS

Silica PQ-ES70X was provided by PQ-Corporation and used as received. $\text{Al}(\text{NO}_3)_3 \cdot 9\text{H}_2\text{O}$ (99.999% trace metals), $\text{Mg}(\text{NO}_3)_2 \cdot 6\text{H}_2\text{O}$ (99.999% trace metals), Na_2CO_3 (anhydrous, 99.999%) NaOH ($>98\%$, pellets) were purchased from Aldrich and used as received.

Silica@LDH Synthesis (See Table S1 for Masses of Reagents, Volumes of Solvents, Addition Rates, Molarity of NaOH Solution and Yields). $\text{Al}(\text{NO}_3)_3 \cdot 9\text{H}_2\text{O}$ was dissolved in D.I. water and added to PQ-ES70X before the powder was dried at $120\text{ }^{\circ}\text{C}$ for 1 h. Na_2CO_3 was dissolved in D.I. water and the silica was suspended in this solution by stirring at 500 rpm and the pH was adjusted to 10 using 4 M HNO_3 or 5 M NaOH . A solution of $\text{Mg}(\text{NO}_3)_2 \cdot 6\text{H}_2\text{O}$ and $\text{Al}(\text{NO}_3)_3 \cdot 9\text{H}_2\text{O}$ in D.I. water was then added at a constant rate, the pH was maintained using NaOH .

After the addition was complete, the suspension was stirred for 1 h. Solids were collected by filtration and washed with D.I. water until the filtrate was neutral. The wet solid was then resuspended in D.I. water and stirred for 1 h (500 rpm). The solids were then collected by filtration, washed with D.I. water until the filtrate was neutral and dried in a vacuum oven at room temperature overnight.

LDH Synthesis (See Table S1 for Masses of Reagents, Volumes of Solvents, Addition Rates, Molarity of NaOH Solution and Yields). Na_2CO_3 was dissolved in D.I. water, stirred at 500 rpm and the pH was adjusted to 10 using 4 M HNO_3 . A solution of $\text{Mg}(\text{NO}_3)_2 \cdot 6\text{H}_2\text{O}$ and $\text{Al}(\text{NO}_3)_3 \cdot 9\text{H}_2\text{O}$ in D.I. water was then added at a constant rate, the pH was maintained using NaOH .

After the addition was complete, the suspension was stirred for 1 h. Solids were collected by filtration and washed with D.I. water until the filtrate was neutral. The wet solid was then resuspended in D.I. water and stirred for 1 h (500 rpm). The solids were then collected by filtration, washed with D.I. water until the filtrate was neutral and dried in a vacuum oven at room temperature overnight.

Calcination. Approximately 800 mg of silica@LDH or 400 mg of LDH was placed in a ceramic crucible, which was then placed in a quartz tube. This tube was placed in a tube furnace, connected to a Schlenk line and evacuated. Once a suitably low vacuum was reached ($<2 \times 10^{-1}$ mbar), the sample was heated to the specified temperature (200 or $400\text{ }^{\circ}\text{C}$) at a heating rate of $10\text{ K}\cdot\text{min}^{-1}$, and this temperature was maintained for 6 h. The tube was under dynamic vacuum throughout the calcination and after calcination the tube was sealed and brought into a glovebox where the calcined supports were stored.

Rehydration and Reconstruction. Approximately 150 mg of calcined material was suspended in 10 mL of Na_2CO_3 solution ($0.08\text{ mol}\cdot\text{L}^{-1}$) and stirred at 500 rpm for 3 h. The reconstructed sample was collected by filtration, washed with D.I. water until the filtrate was neutral and dried in a vacuum oven at room temperature overnight.

Analytical Techniques. Powder X-ray diffraction (PXRD) analysis was carried out using a PANAnalytical X'Pert Pro Diffractometer in scanning mode using $\text{Cu K}\alpha$ radiation ($\alpha_1 = 1.540598\text{ \AA}$, $\alpha_2 = 1.544426\text{ \AA}$) in reflection mode at 40 kV and 40 mA. The samples were packed on stainless steel holders which can result in peaks at 43.36 , 44.29 , and 50.51° but which did not interfere with the analysis. Signals between $2\theta = 2\text{--}70^{\circ}$ were recorded with step size 0.0167° and 40 s per step. To more accurately determine the position of the 110 Bragg reflection of the reconstructed samples, reflections occurring between $2\theta = 55\text{--}65^{\circ}$ were recorded with step size 0.0084° and 150 s per step. Calcined samples were packed in the glovebox and were run immediately after bringing out the glovebox; no evidence of reconstruction was observed.

Particle sizing was carried out using a Malvern Instruments Mastersizer 2000 fitted with a Hydro 2000MU. Samples were dispersed in water using sonication and stirring at 3000 rpm, sufficient sample was added to obscure approximately 1% of the total light. Particles were then measured over the size range 0.020–2000 μm .

Thermogravimetric analyses (TGA) were performed under a nitrogen atmosphere using a PerkinElmer TGA 8000. The weight change was recorded from 30–800 $^{\circ}\text{C}$ (5 $\text{K}\cdot\text{min}^{-1}$). Under these conditions, thermal transitions occur within ± 1.5 $^{\circ}\text{C}$ of the literature values and inaccuracies in the mass recorded are less than 0.02%.

Solid state NMR spectroscopic experiments were run by Dr. Nicholas H. Rees on a Bruker Avance III HD solid state NMR spectrometer equipped with a 9.4 T magnet. Calcined samples were packed in the glovebox to prevent reconstruction. Samples for ^{27}Al DPMAS NMR were packed in 3.2 mm O.D. rotors and spun at 20 kHz. For ^{27}Al in order to obtain quantitative MAS spectra, single pulse excitation was applied using a short pulse length (0.325 μs). Typically 100,000 scans were acquired with a 0.01 s delay. The ^{27}Al chemical shift was externally referenced to an aqueous solution of $\text{Al}(\text{NO}_3)_3$ (0 ppm). For ^{29}Si ssNMR, samples were packed in 4 mm O.D. rotors and spun at 10 kHz. DPMAS spectra were acquired with a one-pulse sequence and spinal64 proton decoupling. Typically 8000 transients were acquired with a recycle delay of 30 s. For CPMAS spectra typically 100 000 scans were acquired with a contact time of 2.5 ms and recycle delay of 0.5 s. All ^{29}Si spectra were externally referenced to kaolinite (taken to be at $\delta = -91.7$ ppm on a scale where $\delta(\text{TMS}) = 0$) as a secondary reference.

Inductively coupled plasma optical emission spectroscopy (ICP-OES) analyses were carried out by Dr. Nigel Howard, Microanalysis, Department of Chemistry, University of Cambridge. ICP-OES was performed on a Thermo Fisher Scientific iCAP 7400 Duo ICP Spectrometer. Calibration was performed by construction of a standard curve using ICP standards from Sigma-Aldrich. Samples were run in $\sim 2\%$ nitric acid (Fisher TraceMetal grade). Samples were weighed on a Mettler UMT2 balance and dissolved in 5 mL nitric acid, diluted with 5 mL water and a 0.5 mL aliquot was diluted to 10 mL with water. For samples containing approximately 4 wt % Al and 6 wt % Mg, there is a total error of $<5\%$ on the values obtained ($<2\%$ measurement error, $<3\%$ sample preparation error).

RESULTS AND DISCUSSION

This study was prompted by our interest in developing silica@LDH as a novel catalyst support technology for polymerization catalysis,⁵⁵ an area where the tunability of LDH has allowed for control of both the catalyst activity and polymer properties.^{56,57} We selected a commercial silica, PQ-ES70X as an appropriate base silica for this study. This silica grade is comprised of much larger agglomerates than those previously used to prepare silica@LDH particles (average diameter, $d_{0.5} = 50$ μm , while previous silicas used range from 40–1000 nm^{19–22,24}), while the surface area (295 $\text{m}^2\cdot\text{g}^{-1}$) is within the range previously reported (17–1000 $\text{m}^2\cdot\text{g}^{-1}$).^{19,21,30} Core-shells were then prepared by coprecipitation at pH 10.¹⁹ To facilitate the deposition of LDH platelets on the silica core, they were first impregnated with aluminum nitrate (0.2 mmol- $\text{g}_{\text{PQ-ES70X}}^{-1}$) before coprecipitation was carried out. The ratio of Mg/Al was set at 2:1 and 3:1 including the aluminum used for impregnation and these core-shells are labeled PQ-

ES70X@ $\text{Mg}_{2.8}\text{Al}$ and PQ-ES70X@ $\text{Mg}_{3.3}\text{Al}$ respectively (where 2.8 and 3.3 correspond to the Mg/Al ratio in the LDH phase alone determined by ICP-OES and PXRD, *vide infra*). For comparison, two LDH samples with coprecipitation ratios of 2:1 and 3:1 were also prepared using the same synthesis conditions only without the silica core ($\text{Mg}_{1.9}\text{Al}$ and $\text{Mg}_{2.8}\text{Al}$ respectively).

XRD powder patterns of the obtained core-shells (Figure 1 for PQ-ES70X@ $\text{Mg}_{2.8}\text{Al}$, Figure S1 for PQ-ES70X@ $\text{Mg}_{3.3}\text{Al}$)

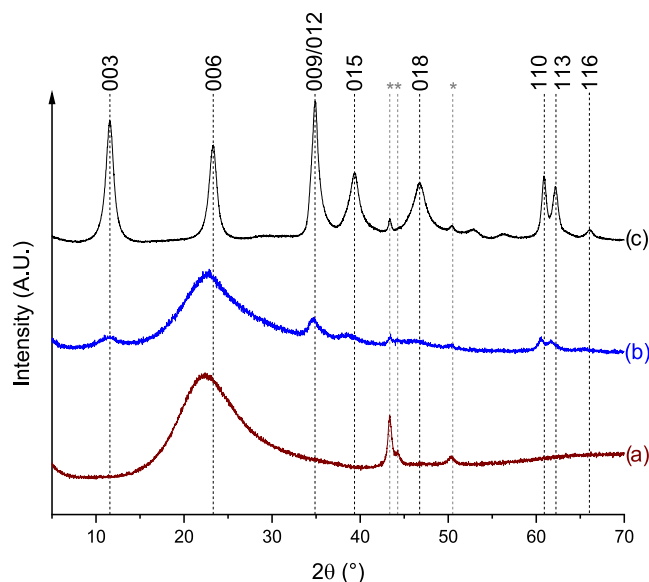


Figure 1. XRD powder patterns of (a) PQ-ES70X (b) PQ-ES70X@ $\text{Mg}_{2.8}\text{Al}$ (c) $\text{Mg}_{1.9}\text{Al}$. Bragg reflections marked with an asterisk arise from the sample holder.

show that phases associated with silica and LDH are formed, however the LDH appears highly disordered particularly along the c axis with only a very weak, very broad 003 Bragg reflection observed. This disorder appears to arise partly from the synthesis conditions, with broad, low intensity 001 Bragg reflections also being observed for the LDH, but this disorder increases for the core-shell samples, suggesting deposition of the platelets on the silica surface competes with the stacking of platelets into layers.

Scanning electron microscopy (SEM) (Figure 2) and light scattering measurements (Figure 3) show that the silica@LDH reflects the base silica in size and shape, forming irregular spheroidal particles with an average diameter of 50 μm with very few particles larger than 100 μm . This is in stark contrast to the free LDH which consists of small particles, which form

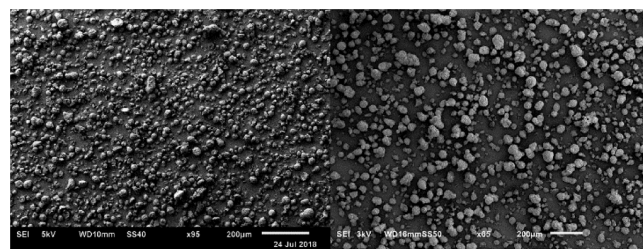


Figure 2. SEM Images of silica, PQ-ES70X (left) and PQ-ES70X@ $\text{Mg}_{2.8}\text{Al}$ (right), showing the size and morphology of the core silica is broadly reproduced in the core-shell.

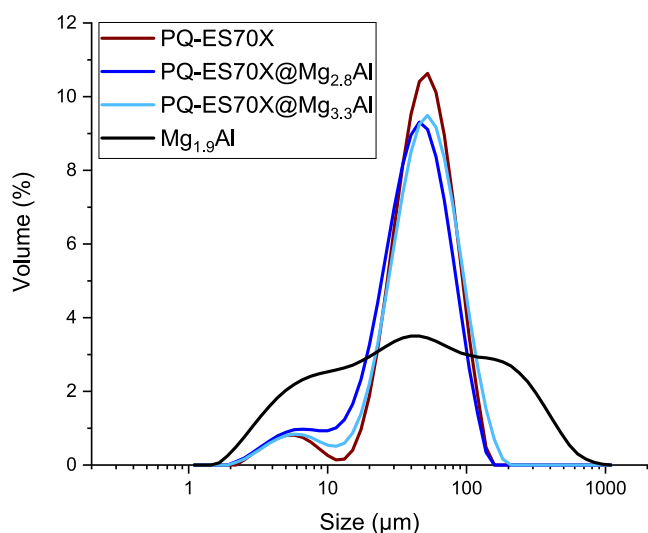


Figure 3. Particle size as determined by laser light-scattering, for PQ-ES70X, PQ-ES70X@Mg_{2.8}Al, PQ-ES70X@Mg_{3.3}Al and Mg_{1.9}Al.

large agglomerates several hundred microns in size leading to a very broad particle size distribution (Table 1).

Table 1. Average Particle Sizes and Size Distributions of Silica, Silica@LDH and LDH Samples as Determined by Light Scattering Measurements

sample	$d(0.1)$ (μm)	$d(0.5)$ (μm)	$d(0.9)$ (μm)	span ^a
PQ-ES70X	23.6	51.2	93.7	1.4
PQ-ES70X@Mg _{2.8} Al	14.5	44.4	87.5	1.6
PQ-ES70X@Mg _{3.3} Al	19.9	51.5	102.1	1.6
Mg _{1.9} Al	6.0	42.9	260.0	5.9

$$^a \text{Span} = [(d(0.9) - d(0.1))/d(0.5)].$$

Thermal analysis (Figure S2) shows that as previously reported,^{19,20} the silica@LDH core-shells show a similar thermal behavior to pristine LDHs, with distinct transitions below 200 and 400 °C corresponding to loss of surface and interlayer water (<200 °C) and the dehydroxylation of the layers and the loss of the interlayer carbonate anions (<400 °C) respectively.^{38–41,43} From the residual weight at 800 °C, the mass of LDH on the original core-shell material can be estimated and is found to be just under 30% which is consistent with the weight of the silica@LDH produced relative to the amount of silica used.

ICP-OES was used to determine the Mg/Al ratio of the synthesized core-shells (see Table S2 for full results). This showed a good agreement with the coprecipitation ratios of 2 and 3 (2.2 and 3.1 respectively), comparable to the unsupported Mg_{1.9}Al and Mg_{2.8}Al-LDHs (1.9 and 2.8 respectively), and within the error range of ICP-OES. No sodium was detected demonstrating that any sodium silicates formed are minimal and are removed on workup of the core-shell product. From the ²⁷Al DPMAS NMR spectrum (see Figures 4 and S3) it is clear that a considerable amount of the aluminum (~35%) is incorporated into an interface layer, forming four-coordinate aluminum ($\text{Al}_{\text{IV}} \approx 55$ ppm) species that are not present in the free LDH, which shows only six-coordinate ($\text{Al}_{\text{VI}} \approx 8$ ppm) species consistent with the octahedra which make up the brucite-like metal hydroxide layers in the LDH.

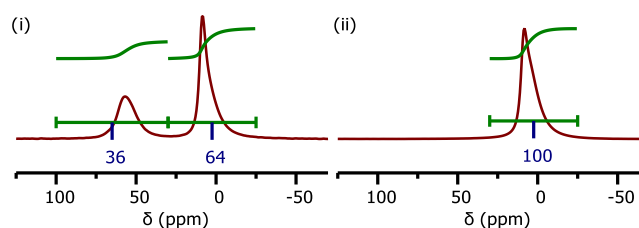


Figure 4. ²⁷Al DPMAS NMR spectrum (20 kHz spinning) of (i) PQ-ES70X@Mg_{2.8}Al and (ii) Mg_{1.9}Al.

The Al_{IV} species detected in the DPMAS NMR spectra are not part of the metal hydroxide layers in the LDH and the removal of aluminum to form this interface will inevitably influence the amount present in the layers. This is also apparent in the XRD powder diffractograms, where there is a clear shift in the 110 Bragg reflection (Figure 5) (which is correlated to the metal–metal distance) from $2\theta = 60.89^\circ$ for Mg_{1.9}Al to 60.39° for PQ-ES70X@Mg_{2.8}Al (see Figure 1). Using the position of the 110 Bragg reflection to determine the unit cell parameter a , and comparing it to Mg_xAl LDH samples of known composition, the Mg/Al ratio of the LDH platelets in the core-shells can be determined with good accuracy (from Mg_{1.9}Al and Mg_{2.8}Al, the error is approximately ± 0.1 , see SI for more details).^{58–60} They were found to be 2.8 (PQ-ES70X@Mg_{2.8}Al, overall ratio of 2.2 by ICP-OES) and 3.3 (PQ-ES70X@Mg_{3.3}Al, overall ratio of 3.1 by ICP-OES), showing how significant the formation of the aluminum-containing interface can be on the composition of the LDH platelets.

As the $\text{M}^{2+}/\text{M}^{3+}$ ratio can have a significant effect on many key properties of an LDH, it is desirable to be able to control the synthesis of silica@LDH samples to produce products with well-defined M/M' ratios. To synthesize a core-shell where the LDH shell consists of platelets with an Mg/Al ratio of 2, a series of silica@LDH were synthesized (Tables 2 and S2). The Mg/Al molar ratio of the metals salt solution added during coprecipitation was fixed at 2:1, while additional $\text{Al}(\text{NO}_3)_3 \cdot 9\text{H}_2\text{O}$ used to impregnate the sample was increased steadily with 0.2, 0.4, 0.48, and 0.6 mmol-gPQ-ES70X^{−1} being used.

From the XRD powder patterns (Figure Si and S4), the LDH Mg/Al ratio can be determined and it can be seen that this decreases linearly with increasing amounts of aluminum impregnation, with 0.48 mmol $\text{Al}(\text{NO}_3)_3 \cdot 9\text{H}_2\text{O}$ allowing for the production of a silica@LDH with the desired Mg/Al ratio of 2.0 (Figure Sii).

Studying the interfacial aluminum species by ²⁷Al DPMAS NMR spectroscopy (Figure S5), it is clear that a consistent amount of aluminum (approximately 0.6 mmol-gPQ-ES70X^{−1}) is used to produce the interface in all silica@LDH, while the additional aluminum is incorporated into the octahedral (Al_{VI}) environment within the LDH platelets (Figure Siii).

This is also supported by TGA analysis, which shows that the residual weight at 800 °C decreases with increasing aluminum impregnation (Figures S6 and S7), suggesting that the weight of the LDH fraction increases (consistent with the incorporation of more aluminum and the associated carbonate anion). While this trend is not perfectly linear, it is affected not only by the composition of the silica@LDH but also by the moisture content both within the pores and on the surface of the particles contributing to the initial weight. Evidence of a changing composition is also seen in the dehydroxylation which takes place between 200 and 400 °C (Figure 6). This

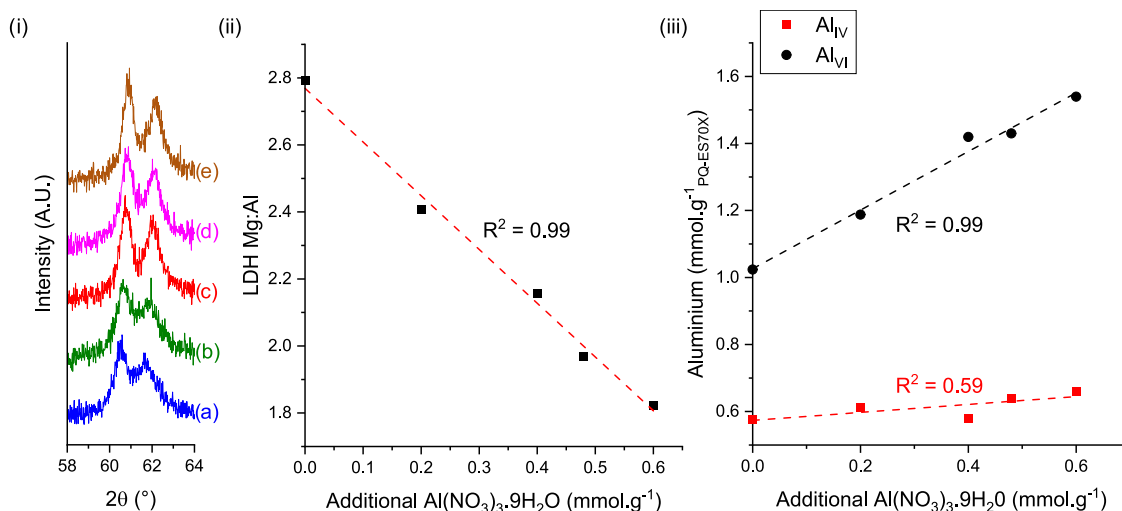


Figure 5. (i) XRD powder patterns between $2\theta = 58$ and 64° , for (a) PQ-ES70X@Mg_{2.4}Al, (b) PQ-ES70X@Mg_{2.2}Al, (c) PQ-ES70X@Mg_{2.0}Al, (d) PQ-ES70X@Mg_{1.8}Al and (e) PQ-ES70X@Mg_{1.6}Al. (ii) Change in LDH Mg/Al ratio with additional aluminum impregnation as determined from the unit cell, a , derived from the position of the 110 Bragg reflection ($a = 2(d_{110})$). (iii) Distribution of aluminum present in silica@LDH as Al_{IV} (100 to 30 ppm) and Al_{VI} (30 to −25 ppm) sites, showing the change in Al_{VI} sites with increasing Al(NO₃)₃·9H₂O impregnation.

Table 2. Silica@LDH Samples Produced to Study the Effect of Aluminum Impregnation on Mg/Al

sample	additional aluminum used (mmol.g ⁻¹)	Mg/Al (ICP-OES)	Mg/Al (XRD) ^a
PQ-ES70X@Mg _{2.4} Al	0.20	1.74	2.41
PQ-ES70X@Mg _{2.2} Al	0.40	1.59	2.16
PQ-ES70X@Mg _{2.0} Al	0.48	1.51	1.97
PQ-ES70X@Mg _{1.8} Al	0.60	1.44	1.82

^aDetermined from the position of the 110 Bragg reflection.

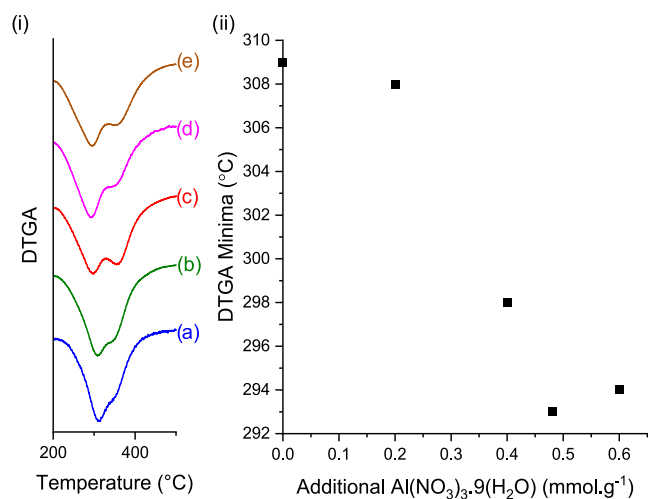


Figure 6. (i) dTGA between 200 and 500 °C of (a) PQ-ES70X@Mg_{2.4}Al, (b) PQ-ES70X@Mg_{2.2}Al, (c) PQ-ES70X@Mg_{2.0}Al, (d) PQ-ES70X@Mg_{1.8}Al and (e) PQ-ES70X@Mg_{1.6}Al. (ii) Position of dTGA minima with additional aluminum impregnation. For full dTGA see Figure S8.

transition corresponds to the loss of hydroxyl groups shared between three metal cations, M₃(OH), and is highly dependent on the nature of those metal ions, with Mg₃(OH) units decomposing at a higher temperature than Mg₂Al(OH) units.^{40,41} The dTGA minima move to lower temperature with increasing aluminum impregnation, reflective of a higher

percentage of Mg₂Al(OH) units in the layers. While this shift in the dTGA minima from 309 to 293 °C is not linear, it is influenced by the surrounding peaks including a second smaller minima above 350 °C, which can be tentatively assigned to the dehydroxylation of Mg₃(OH) units. These will form even in LDH layers with an Mg/Al ratio of 2 as the short aging time of the synthesis will lead to a disordered cation distribution with MgAl₂(OH), Mg₂Al(OH) and Mg₃(OH) units,^{61,62} despite the well documented preference for arrangements that limit adjacent aluminum octahedra.^{62–66}

Clearly this interface significantly influences the chemical composition of the LDH platelets. While the interface has previously been proposed to consist of Si–O–Al and Si–O–Mg bonds, the effect that the interface has on the Mg/Al ratio of the platelets and the formation of a consistent amount of interfacial aluminum (Al_{IV}), strongly suggests that the interface is preferentially and primarily formed from Si–O–Al bonds. However, the presence of magnesium in the interface cannot be completely ruled out. PQ-ES70X@Mg_{3.3}Al contains less interfacial aluminum (0.44 mmol.g⁻¹) than expected, and the ratio of Al_{VI} to Mg is significantly higher (5.0) than the value determined by XRD (3.3). Therefore, it is possible that some Mg can be incorporated into the interface, which might also explain the relatively small difference between the theoretical Mg/Al ratio and the ratio determined by XRD for PQ-ES70X@Mg_{3.3}Al. Attempts to observe magnesium in the interface using ²⁵Mg DPMAS NMR spectroscopy were unsuccessful, presumably due to the low natural abundance and sensitivity of this nucleus.

Further attempts to study the interface were made using ²⁹Si MAS NMR spectroscopy. ²⁹Si DPMAS NMR spectra (Figure 7i) of these silica@LDH core–shells are dominated by the resonance at −112 ppm which can be assigned to the Q⁴ Si atom (Si(OSiO₃)₄).⁶⁷ This resonance is associated with the silica core rather than the silica surface, where the interface is formed. To observe the surface, ²⁹Si CPMAS NMR spectroscopy was used (Figure 7ii–iv). In this experiment the sensitivity of ²⁹Si NMR spectroscopic signals are enhanced depending on whether there are nearby protons. This provides a more detailed spectrum, with the most significant resonance

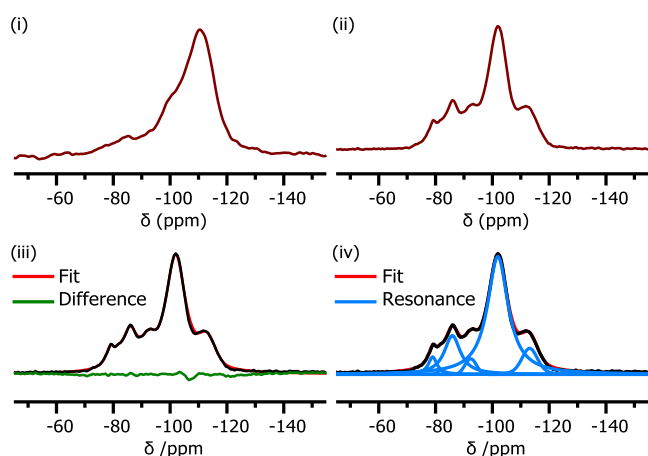


Figure 7. (i) ^{29}Si DPMAS and (ii) ^{29}Si CPMAS NMR spectra of PQ-ES70X@Mg_{3.3}Al, (iii) fitting of ^{29}Si CPMAS NMR spectrum of PQ-ES70X@Mg_{3.3}Al, showing the fit and the difference between the measured and simulated spectra, (iv) deconvolution of simulated fit into six resonances. See Tables S3 and S4, and Figure S9 for assignment of the different resonances and Figures S10–S17 for ^{29}Si CPMAS NMR spectra of all silica@LDH samples.

being that of the Q³ silanol ($\text{Si}(\text{OH})(\text{OSiO}_3)_3$) at -102 ppm, while a resonance associated with the Q² (geminal) silanol ($\text{Si}(\text{OH})_2(\text{OSiO}_3)_2$) is visible at -93 ppm.⁶⁷ The Q₄ Si resonance is still visible, but greatly reduced. There are also additional resonances at -79 , -83 and -86 ppm. While these resonances could be generated by Si–O–Mg linkages, as has been observed by impregnation of silica with Mg(II)⁶⁸ and in magnesium silicate hydrates,⁶⁹ they can also be adequately explained by formation of a silica–alumina interface.⁷⁰ The silica–alumina interface model can also account for all the ^{29}Si resonances without requiring the generation of Q¹ species,²¹ or species with very high substitution of silicon with aluminum such as Q⁴(4Al) ($\text{Si}(\text{OAlO}_3)_4$).⁷¹ This is because at a silica–alumina interface, higher coordination of oxygen is possible than in silica due to the more ionic character of alumina.⁷⁰

To show that the interface can be formed in the absence of magnesium, an attempt was made to approximate the formation of the interface in the absence of LDH by impregnating the silica core with $\text{Al}(\text{NO}_3)_3 \cdot 9\text{H}_2\text{O}$ and treating with a solution of sodium carbonate. When 0.48 mmol of $\text{Al}(\text{NO}_3)_3 \cdot 9\text{H}_2\text{O}$ is used to impregnate 1.0 g of silica, the ^{29}Si CPMAS NMR spectrum is quite comparable to PQ-ES70X@Mg_{2.0}Al which is also impregnated with the same amount of aluminum nitrate (Figure 8ii,iv). The ^{27}Al DPMAS spectra contain the expected Al_{IV} resonance (see Figure 8i,iii). TGA shows that the aluminum species formed is thermally stable up to 800 °C, which is consistent with formation of alumina, and not aluminum hydroxide (see Figures S17 and S18). The PXRD pattern of the impregnated silica contains no additional reflections compared to silica, which is consistent with the interfacial aluminum species not being observed by PXRD (see Figure S19).

For alumina in a silica–alumina interface, it would be expected that Al_{VI} and penta-coordinated aluminum (Al_{V}) species would also be present, rather than just Al_{IV} species.⁷⁰ However, the aluminum content of this interface is very low (maximum 0.6 mmol Al, or 2.9 wt % Al_2O_3 at the highest impregnation level of 0.6 mmol \cdot g^{−1} $\text{Al}(\text{NO}_3)_3 \cdot 9\text{H}_2\text{O}$) and in

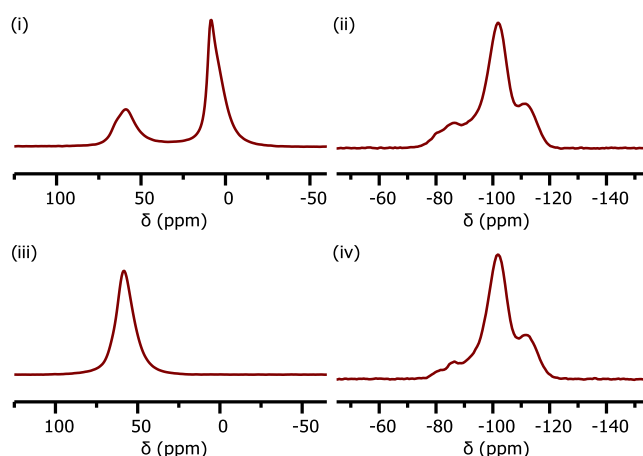


Figure 8. (i) ^{27}Al DPMAS and (ii) ^{29}Si CPMAS NMR spectra of PQ-ES70X@Mg_{2.0}Al, (iii) ^{27}Al DPMAS and (iv) ^{29}Si CPMAS NMR spectra of PQ-ES70X impregnated with 0.48 mmol of $\text{Al}(\text{NO}_3)_3 \cdot 9\text{H}_2\text{O}$.

the region where only Al_{IV} was found in amorphous silica–alumina catalysts produced by dealumination.⁷²

It therefore seems likely that the interface is a thin, amorphous layer of alumina dominated by Al^{IV} sites, due to the higher stability of these species and the solubility of alumina at the high synthesis pH, leading to both deposition and dissolution of aluminum species under these conditions.⁷³

After calcination of the parent LDH Mg_{1.9}Al and silica@LDH samples to 200 °C, the XRD patterns (see Figure S20) show that the layered structure remains, albeit considerably disordered, consistent with dehydration but not dehydroxylation of the sample. ^{27}Al DPMAS NMR spectroscopy of calcined Mg_{1.9}Al (Figure 9a) shows the formation of an Al_{IV}

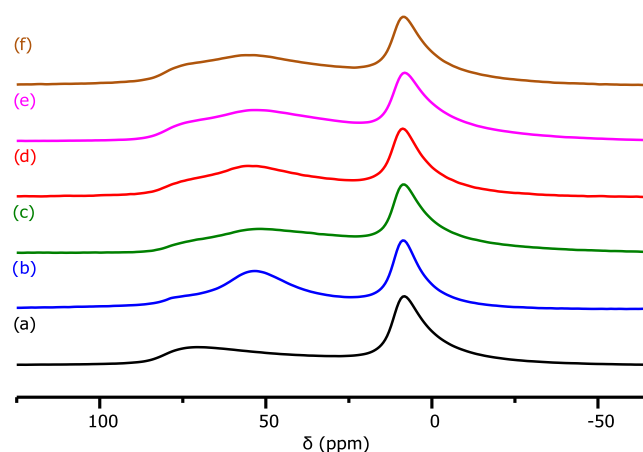


Figure 9. ^{27}Al DPMAS NMR spectra of calcined (200 °C) samples of (a) Mg_{1.9}Al (b) PQ-ES70X@Mg_{2.8}Al (c) PQ-ES70X@Mg_{2.4}Al (d) PQ-ES70X@Mg_{2.2}Al (e) PQ-ES70X@Mg_{2.0}Al and (f) PQ-ES70X@Mg_{1.8}Al, showing an Al_{VI} species (11 ppm) and two Al_{V} species (75 and 55 ppm) after calcination to 200 °C.

species after calcination, located at ≈ 75 ppm distinct from the interfacial species in silica@LDH (≈ 55 ppm) which corresponds to the previously reported interlayer species.⁷⁴ ^{27}Al DPMAS NMR spectroscopy of the calcined silica@LDH samples show both these Al_{IV} species (at 75 and 55 ppm) are present (Figure 9b–f). For all silica@LDH samples, the position of the Al_{IV} species at 55 ppm and the Al_{VI} species are

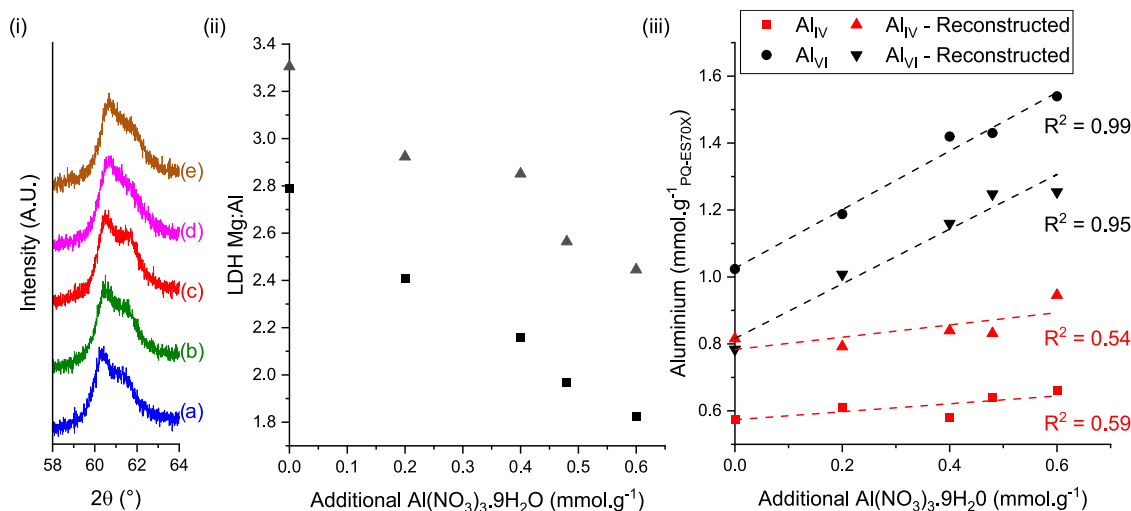


Figure 10. (i) XRD powder patterns between $2\theta = 58$ and 64° , for (a) PQ-ES70X@Mg_{2.8}Al, (b) PQ-ES70X@Mg_{2.4}Al, (c) PQ-ES70X@Mg_{2.2}Al, (d) PQ-ES70X@Mg_{2.0}Al and (e) PQ-ES70X@Mg_{1.8}Al after calcination to 200°C and reconstruction with Na₂CO₃ solution. (ii) Change in Mg/Al ratio with additional aluminum impregnation as determined from the unit cell, a , derived from the position of the 110 Bragg reflection ($a = 2(d_{110})$) before (■) and after (▲) calcination at 200°C and reconstruction with Na₂CO₃ solution. For full powder patterns of reconstructed samples see (Figure S23). (iii) Change in proportion of aluminum present in the silica@LDH as six-coordinate (Al_{VI}) and four-coordinate (Al_{IV}) species before and after calcination to 200°C and reconstruction with Na₂CO₃ solution.

relatively unchanged during the calcination process. While ²⁹Si CPMAS NMR spectroscopy allows direct observation of the interface, it is reliant on the presence of protons; after calcination the dehydration of the LDH and condensation of surface silanols to siloxanes meant useful information on the interface could not be obtained for calcined samples (Figure S21).

After rehydrating the samples calcined at 200°C , XRD, TGA and ²⁷Al DPMAS NMR spectra of LDH and silica@LDH show that the migration of aluminum has not been completely reversed. From the ²⁷Al DPMAS NMR spectrum (Figure S22), approximately 10% of the aluminum in Mg_{1.9}Al remains as Al_{IV}, with comparable change in the aluminum distribution for silica@LDH. The amount of aluminum impregnation does not influence the degree of reconstruction, with a consistent increase in Mg/Al ratio (as determined by XRD, Figure 10ii) and Al_{IV} (from $0.6 \text{ mmol} \cdot \text{g}_{\text{PQ-ES70X}}^{-1}$ to approximately $0.8 \text{ mmol} \cdot \text{g}_{\text{PQ-ES70X}}^{-1}$, Figure 10iii) for all samples.

Similar trends are seen in the TGA with a decrease in the residual weight and an increase in the dTGA minima, consistent with a change in the composition of LDH layers to include more Mg₃(OH) units (see Figures S24–S30). Despite these indicators of a loss of aluminum, ICP-OES suggests the magnesium and aluminum content and therefore the overall Mg/Al ratio remains constant (see Tables S5–S7), implying that the aluminum has not been lost in the reconstruction process but has migrated from the LDH layers to the silica–alumina interface.

Further calcination to 400°C , is associated with the formation of layered double oxide (LDO). This involves significant migration of aluminum ions with predominantly Al_{IV} being present after calcination (Figure S31). Reconstruction of these species shows a significant difference between silica@LDH and LDH. While this migration of aluminum ions is almost completely reversible in LDH (as shown by XRD and ²⁷Al DPMAS NMR spectra, see Figures S32 and S33), a significant proportion of the aluminum is retained as Al_{IV} species in silica@LDH (Figure 11i,ii) increasing from 0.6 to

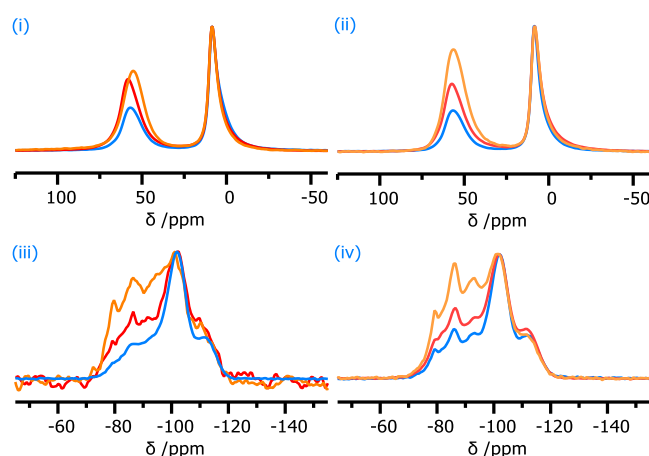


Figure 11. ²⁷Al DPMAS NMR spectra of (i) PQ-ES70X@Mg_{2.8}Al and (ii) PQ-ES70X@Mg_{3.3}Al and ²⁹Si CPMAS NMR spectra of (iii) PQ-ES70X@Mg_{2.8}Al and (iv) PQ-ES70X@Mg_{3.3}Al samples before calcination (blue), after calcination to 200°C and reconstruction (red) and after calcination to 400°C and reconstruction (orange).

$0.9 \text{ mmol} \cdot \text{g}^{-1}$ for PQ-ES70X@Mg_{2.8}Al. The reconstructed samples can also be compared using XRD. The 110 and 113 Bragg reflections are broader for the reconstructed LDH compared to the pristine samples (see Figure S34), presumably due to a reduction in crystallite domain length upon reconstruction.⁷⁵ The position of the 110 reflection is shifted but reflects the Mg/Al ratios of the initial sample, 1.6 for Mg_{1.9}Al and 2.5 for Mg_{2.8}Al. However, the reconstructed silica@LDH samples are significantly different, the 110 and 113 reflections have shifted to a lower 2θ values and can no longer be resolved, making an accurate estimation of the LDH Mg/Al ratio impossible, though it can be assumed to be higher than the initial ratios of 2.8 and 3.3. A similar trend is observed in the TGA, with a shift in the dTGA minima of silica@LDH to higher temperatures consistent with a higher Mg/Al ratio (Figures S35–S37).

While the LDH layer has clearly lost aluminum, the ICP-OES values suggest that the overall ratio remains relatively constant, suggesting that the aluminum is not lost but has irreversibly migrated to the interface. This is also supported by the growth of both the Al^{IV} resonance in the ^{27}Al DPMAS spectra (Figure 11i,ii) and the growth of resonances associated with the interface in the ^{29}Si CPMAS NMR spectra (Figure 11iii,iv).

From these results it is clear that upon calcination of silica@LDH there is a migration of aluminum ions out of the layers, and into the silica–alumina interface. In contrast to the interlayer species observed upon calcination of LDH, this process demonstrates little reversibility and compared to the slow segregation into spinel- and binary oxide phases observed for LDH (which requires multiple cycles of calcination and reconstruction) and significantly impacts the LDH composition.

CONCLUSIONS

While extensive attention has been paid to the control of morphology for core–shell silica@LDH composite materials, until now little emphasis has been paid to how formation of the core–shell structure influences the tunable composition of the LDH layers. Typically, it has been assumed that the interface observed contains both magnesium and aluminum, and that the composition of the LDH shell is relatively unaffected. However, this study finds that the interface is more consistent with a silica–alumina species, the formation of the interface consumes a significant amount of aluminum used in the synthesis of LDH and the composition of the LDH platelets is significantly altered from the free LDH. However, the interface formation can be accounted for by increasing the amount of aluminum used to form the silica@LDH where the LDH have the desired Mg/Al ratio.

Upon calcination there is a significant migration of aluminum ions into the silica–alumina interface. In stark contrast to the relatively reversible formation of LDO, this incorporation into the interface is permanent and significantly influences the composition of the LDH shell after just a single cycle of calcination and reconstruction. Longer reconstruction times may improve this but are hindered due to the competing dissolution of the silica-core. These two factors means that there is a significant challenge to be overcome in preparing silica@LDH composites with fixed M(II)/M(III) ratios, particularly if a calcination step is required either for the application or to introduce a specific anion. An enhanced understanding of the nature of the interface that exists in silica@LDH core–shell materials and the role it plays in the composition of the LDH itself now affords more rational design in these core–shell systems, enabling them to be better tailored to specific applications. This approach to interrogate the chemical composition of LDH in core–shell systems via multiple techniques can now be translated to other core@LDH systems used in catalysis and other applications.

ASSOCIATED CONTENT

Supporting Information

The Supporting Information is available free of charge at <https://pubs.acs.org/doi/10.1021/acs.jpcc.4c02999>.

Additional synthetic details, XRD patterns, ICP-MS analysis, solid state NMR spectra, TGA data (PDF)

AUTHOR INFORMATION

Corresponding Author

Dermot O'Hare – Chemistry Research Laboratory,
Department of Chemistry, University of Oxford, Oxford OX1
3TA, U.K.; orcid.org/0000-0001-8054-8751;
Email: dermot.ohare@chem.ox.ac.uk

Authors

Philip Kenyon – Chemistry Research Laboratory, Department
of Chemistry, University of Oxford, Oxford OX1 3TA, U.K.;
orcid.org/0000-0003-0244-1347

Samuel Roberts – Chemistry Research Laboratory,
Department of Chemistry, University of Oxford, Oxford OX1
3TA, U.K.

Zoë R. Turner – Chemistry Research Laboratory, Department
of Chemistry, University of Oxford, Oxford OX1 3TA, U.K.;
orcid.org/0000-0003-2044-9203

Nicholas H. Rees – Chemistry Research Laboratory,
Department of Chemistry, University of Oxford, Oxford OX1
3TA, U.K.

Complete contact information is available at:
<https://pubs.acs.org/10.1021/acs.jpcc.4c02999>

Author Contributions

The manuscript was written through contributions of all authors. All authors have given approval to the final version of the manuscript.

Funding

SCG Chemicals Public Co. Ltd. (Thailand)

Notes

The authors declare no competing financial interest.

ACKNOWLEDGMENTS

All authors would like to thank SCG Chemicals Public Co. Ltd (Thailand) for funding and Chemical Crystallography for use of the diffractometers.

REFERENCES

- (1) Cavani, F.; Trifirò, F.; Vaccari, A. Hydrotalcite-type anionic clays: Preparation, properties and applications. *Catal. Today* **1991**, *11* (2), 173–301.
- (2) Laipan, M.; Yu, J.; Zhu, R.; Zhu, J.; Smith, A. T.; He, H.; O'Hare, D.; Sun, L. Functionalized layered double hydroxides for innovative applications. *Mater. Horiz.* **2020**, *7* (3), 715–745.
- (3) Johnston, A.-L.; Lester, E.; Williams, O.; Gomes, R. L. Understanding Layered Double Hydroxide properties as sorbent materials for removing organic pollutants from environmental waters. *J. Environ. Chem. Eng.* **2021**, *9* (4), No. 105197, DOI: [10.1016/j.jece.2021.105197](https://doi.org/10.1016/j.jece.2021.105197).
- (4) Li, X.; Du, D.; Zhang, Y.; Xing, W.; Xue, Q.; Yan, Z. Layered double hydroxides toward high-performance supercapacitors. *J. Mater. Chem. A* **2017**, *5* (30), 15460–15485.
- (5) Xu, M.; Wei, M. Layered Double Hydroxide-Based Catalysts: Recent Advances in Preparation, Structure, and Applications. *Adv. Funct. Mater.* **2018**, *28* (47), No. 1802943, DOI: [10.1002/adfm.201802943](https://doi.org/10.1002/adfm.201802943).
- (6) Prinetto, F.; Ghiotti, G.; Durand, R.; Tichit, D. Investigation of Acid-Base Properties of Catalysts Obtained from Layered Double Hydroxides. *J. Phys. Chem. B* **2000**, *104* (47), 11117–11126.
- (7) Bing, W.; Wei, M. Recent advances for solid basic catalysts: Structure design and catalytic performance. *J. Solid State Chem.* **2019**, *269*, 184–194.
- (8) Gong, M.; Li, Y.; Wang, H.; Liang, Y.; Wu, J. Z.; Zhou, J.; Wang, J.; Regier, T.; Wei, F.; Dai, H. An advanced Ni-Fe layered double

hydroxide electrocatalyst for water oxidation. *J. Am. Chem. Soc.* **2013**, *135* (23), 8452–8455.

(9) Anantharaj, S.; Karthick, K.; Kundu, S. Evolution of layered double hydroxides (LDH) as high performance water oxidation electrocatalysts: A review with insights on structure, activity and mechanism. *Mater. Today Energy* **2017**, *6*, 1–26.

(10) Sahoo, D. P.; Das, K. K.; Mansingh, S.; Sultana, S.; Parida, K. Recent progress in first row transition metal Layered double hydroxide (LDH) based electrocatalysts towards water splitting: A review with insights on synthesis. *Coord. Chem. Rev.* **2022**, *469*, No. 214666, DOI: 10.1016/j.ccr.2022.214666.

(11) Silva, C. G.; Bouizi, Y.; Fornes, V.; Garcia, H. Layered double hydroxides as highly efficient photocatalysts for visible light oxygen generation from water. *J. Am. Chem. Soc.* **2009**, *131* (38), 13833–13839.

(12) Kim, K.-H.; Kim, S.; Moon, B. C.; Choi, J. W.; Jeong, H. M.; Kwon, Y.; Kwon, S.; Choi, H. S.; Kang, J. K. Quadruple metal-based layered structure as the photocatalyst for conversion of carbon dioxide into a value added carbon monoxide with high selectivity and efficiency. *J. Mater. Chem. A* **2017**, *5* (18), 8274–8279.

(13) Zhao, Y.; Jia, X.; Waterhouse, G. I. N.; Wu, L.-Z.; Tung, C.-H.; O'Hare, D.; Zhang, T. Layered Double Hydroxide Nanostructured Photocatalysts for Renewable Energy Production. *Adv. Energy Mater.* **2016**, *6* (6), No. 1501974.

(14) Bomeriame, H.; Da Silva, E. S.; Cherevan, A. S.; Chafik, T.; Faria, J. L.; Eder, D. Layered double hydroxide (LDH)-based materials: A mini-review on strategies to improve the performance for photocatalytic water splitting. *J. Energy Chem.* **2022**, *64*, 406–431.

(15) Khan, A. A.; Tahir, M.; Khan, N. LDH-based nanomaterials for photocatalytic applications: A comprehensive review on the role of bi/trivalent cations, anions, morphology, defect engineering, memory effect, and heterojunction formation. *J. Energy Chem.* **2023**, *84*, 242–276.

(16) Chen, C.; Yang, M.; Wang, Q.; Buffet, J.-C.; O'Hare, D. Synthesis and characterisation of aqueous miscible organic-layered double hydroxides. *J. Mater. Chem. A* **2014**, *2* (36), 15102–15110.

(17) Ruengkajorn, K.; Erastova, V.; Buffet, J.-C.; Greenwell, H. C.; O'Hare, D. Aqueous immiscible layered double hydroxides: synthesis, characterisation and molecular dynamics simulation. *Chem. Commun.* **2018**, *54* (35), 4394–4397.

(18) Leung, D. W. J.; Chen, C.; Buffet, J. C.; O'Hare, D. Correlations of acidity-basicity of solvent treated layered double hydroxides/oxides and their CO₂ capture performance. *Dalton Trans.* **2020**, *49* (27), 9306–9311.

(19) Chen, C.; Felton, R.; Buffet, J.-C.; O'Hare, D. Core-shell SiO₂@LDHs with tuneable size, composition and morphology. *Chem. Commun.* **2015**, *51* (16), 3462–3465.

(20) Kwok, W. L. J.; Crivoi, D. G.; Chen, C.; Buffet, J.-C.; O'Hare, D. Silica@layered double hydroxide core-shell hybrid materials. *Dalton Trans.* **2018**, *47* (1), 143–149.

(21) Shirotori, M.; Nishimura, S.; Ebitani, K. Fine-crystallized LDHs prepared with SiO₂ spheres as highly active solid base catalysts. *J. Mater. Chem. A* **2017**, *5* (15), 6947–6957.

(22) Shirotori, M.; Nishimura, S.; Ebitani, K. Effect of SiO₂ amount on heterogeneous base catalysis of SiO₂@Mg–Al layered double hydroxide. *RSC Adv.* **2018**, *8* (49), 28024–28031.

(23) Wang, K.; Huang, X.; Liu, Y.; Fei, W.; Gu, Z. Different morphologies of SiO₂@Mg–Al-LDH nanocomposites as catalyst for the synthesis of propylene glycol methyl ether. *J. Nanopart. Res.* **2020**, *22* (5), No. 126, DOI: 10.1007/s11051-020-04868-w.

(24) Kondratowicz, T.; Slang, S.; Dubnová, L.; Kikhyanin, O.; Bělina, P.; Čapek, L. Controlled silica core removal from SiO₂@MgAl core-shell system as a tool to prepare well-oriented and highly active catalysts. *Appl. Clay. Sci.* **2022**, *216*, No. 106365, DOI: 10.1016/j.clay.2021.106365.

(25) Ji, X.; Zhang, W.; Shan, L.; Tian, Y.; Liu, J. Self-assembly preparation of SiO₂@Ni–Al layered double hydroxide composites and their enhanced electrorheological characteristics. *Sci. Rep.* **2016**, *5*, No. 18367.

(26) Li, M.; Yuan, P.; Guo, S.; Liu, F.; Cheng, J. P. Design and synthesis of Ni–Co and Ni–Mn layered double hydroxides hollow microspheres for supercapacitor. *Int. J. Hydrogen Energy* **2017**, *42* (48), 28797–28806.

(27) Chen, C.; Wang, P.; Lim, T.-T.; Liu, L.; Liu, S.; Xu, R. A facile synthesis of monodispersed hierarchical layered double hydroxide on silica spheres for efficient removal of pharmaceuticals from water. *J. Mater. Chem. A* **2013**, *1* (12), 3877–3880.

(28) Yang, D.; Song, S.; Zou, Y.; Wang, X.; Yu, S.; Wen, T.; Wang, H.; Hayat, T.; Alsaedi, A.; Wang, X. Rational design and synthesis of monodispersed hierarchical SiO₂@layered double hydroxide nanocomposites for efficient removal of pollutants from aqueous solution. *Chem. Eng. J.* **2017**, *323*, 143–152.

(29) Li, C.; Wei, Y.; Wang, X.; Yin, X. Efficient and rapid adsorption of iodide ion from aqueous solution by porous silica spheres loaded with calcined Mg–Al layered double hydroxide. *J. Taiwan Inst. Chem. Eng.* **2018**, *85*, 193–200.

(30) Suo, H.; Duan, H.; Chen, C.; Buffet, J.-C.; O'Hare, D. Bifunctional acid–base mesoporous silica@aqueous miscible organic-layered double hydroxides. *RSC Adv.* **2019**, *9* (7), 3749–3754.

(31) Cosano, D.; Esquivel, D.; Puertas, A. J.; Romero-Salguero, F. J.; Jiménez-Sanchidrián, C.; Ruiz, J. R. Microstructural analysis of 3D hierarchical composites of hydrotalcite-coated silica microspheres. *Microporous Mesoporous Mater.* **2021**, *323*, No. 111247.

(32) Suo, H.; Chen, C.; Buffet, J. C.; O'Hare, D. Dendritic silica@aqueous miscible organic-layered double hydroxide hybrids. *Dalton Trans.* **2018**, *47* (46), 16413–16417.

(33) Valente, J. S.; Hernandez-Cortez, J.; Cantu, M. S.; Ferrat, G.; López-Salinas, E. Calcined layered double hydroxides Mg–Me–Al (Me: Cu, Fe, Ni, Zn) as bifunctional catalysts. *Catal. Today* **2010**, *150* (3–4), 340–345.

(34) Santos, R. M. M.; Tronto, J.; Briois, V.; Santilli, C. V. Thermal decomposition and recovery properties of ZnAl–CO₃ layered double hydroxide for anionic dye adsorption: insight into the aggregative nucleation and growth mechanism of the LDH memory effect. *J. Mater. Chem. A* **2017**, *5* (20), 9998–10009.

(35) Benhiti, R.; Ichou, A. A.; Aboussabek, A.; Carja, G.; Zerbet, M.; Sinan, F.; Chiban, M. Efficient removal of Cr (VI) from aqueous solution using memory effect property of layered double hydroxide material. *Chemosphere* **2023**, *341*, No. 140127.

(36) Xiong, W.; Wang, J.; Kong, X.; Waterhouse, G. I. N.; Liu, H.; Wang, Y.; Liu, S.; Wang, Y.; Li, S.; Zhao, Y.; Duan, H. Efficient and Superstable Mineralization of Toxic Cd²⁺ Ions through Defect Engineering in Layered Double Hydroxide Nanosheets. *J. Phys. Chem. C* **2023**, *127* (18), 8759–8769.

(37) Chibwe, K.; Jones, W. Synthesis of polyoxometalate pillared layered double hydroxides via calcined precursors. *Chem. Mater.* **1989**, *1* (5), 489–490.

(38) Hudson, M. J.; Carlino, S.; Apperley, D. C. Thermal conversion of a layered (Mg/Al) double hydroxide to the oxide. *J. Mater. Chem.* **1995**, *5* (2), 323–329.

(39) Bellotto, M.; Rebours, B.; Clause, O.; Lynch, J.; Bazin, D.; Elkaïm, E. Hydrotalcite Decomposition Mechanism: A Clue to the Structure and Reactivity of Spinel-like Mixed Oxides. *J. Phys. Chem. A* **1996**, *100* (20), 8535–8542.

(40) Yang, W.; Kim, Y.; Liu, P. K. T.; Sahimi, M.; Tsotsis, T. T. A study by in situ techniques of the thermal evolution of the structure of a Mg–Al–CO₃ layered double hydroxide. *Chem. Eng. Sci.* **2002**, *57* (15), 2945–2953.

(41) Yu, G. Y.; Zhou, Y. H.; Yang, R.; Wang, M.; Shen, L.; Li, Y. H.; Xue, N. H.; Guo, X. F.; Ding, W. P.; Peng, L. M. Dehydration and Dehydroxylation of Layered Double Hydroxides: New Insights from Solid-State NMR and FT-IR Studies of Deuterated Samples. *J. Phys. Chem. C* **2015**, *119* (22), 12325–12334.

(42) Jin, L.; Zhou, X.; Wang, F.; Ning, X.; Wen, Y.; Song, B.; Yang, C.; Wu, D.; Ke, X.; Peng, L. Insights into memory effect mechanisms of layered double hydroxides with solid-state NMR spectroscopy. *Nat. Commun.* **2022**, *13* (1), No. 6093.

- (43) Millange, F.; Walton, R. I.; O'Hare, D. Time-resolved in situ X-ray diffraction study of the liquid-phase reconstruction of Mg–Al–carbonate hydrotalcite-like compounds. *J. Mater. Chem.* **2000**, *10* (7), 1713–1720.
- (44) Mascolo, G.; Mascolo, M. C. On the synthesis of layered double hydroxides (LDHs) by reconstruction method based on the "memory effect". *Microporous Mesoporous Mater.* **2015**, *214*, 246–248.
- (45) Rocha, J.; del Arco, M.; Rives, V.; Ulibarri, M. A. Reconstruction of layered double hydroxides from calcined precursors: a powder XRD and ^{27}Al MAS NMR study. *J. Mater. Chem.* **1999**, *9* (10), 2499–2503.
- (46) Vyalikh, A.; Costa, F. R.; Wagenknecht, U.; Heinrich, G.; Massiot, D.; Scheler, U. From Layered Double Hydroxides to Layered Double Hydroxide-Based Nanocomposites—A Solid-State NMR Study. *J. Phys. Chem. C* **2009**, *113* (51), 21308–21313.
- (47) Valente, J. S.; Lima, E.; Toledo-Antonio, J. A.; Cortes-Jacome, M. A.; Lartundo-Rojas, L.; Montiel, R.; Prince, J. Comprehending the Thermal Decomposition and Reconstruction Process of Sol–Gel MgAl Layered Double Hydroxides. *J. Phys. Chem. C* **2010**, *114* (5), 2089–2099.
- (48) Pfeiffer, H.; Martínez-dlCruz, L.; Lima, E.; Flores, J.; Vera, M. A.; Valente, J. S. Influence of Mg/Al Ratio on the Thermokinetic Rehydration of Calcined Mg–Al Layered Double Hydroxides. *J. Phys. Chem. C* **2010**, *114* (18), 8485–8492.
- (49) van Bokhoven, J. A.; Roelofs, J. C. A. A.; de Jong, K. P.; Koningsberger, D. C. Unique Structural Properties of the Mg–Al Hydrotalcite Solid Base Catalyst: An In Situ Study Using Mg and Al K-Edge XAFS during Calcination and Rehydration. *Chem. - Eur. J.* **2001**, *7* (6), 1258–1265.
- (50) Hibino, T.; Tsunashima, A. Characterization of Repeatedly Reconstructed Mg–Al Hydrotalcite-like Compounds: Gradual Segregation of Aluminum from the Structure. *Chem. Mater.* **1998**, *10* (12), 4055–4061.
- (51) Ferreira, O. P.; Alves, O. L.; Gouveia, D. X.; Filho, A. G. S.; de Paiva, J. A. C.; Filho, J. M. Thermal decomposition and structural reconstruction effect on Mg–Fe-based hydrotalcite compounds. *J. Solid State Chem.* **2004**, *177* (9), 3058–3069.
- (52) Pérez-Ramírez, J.; Abelló, S.; van der Pers, N. M. Influence of the Divalent Cation on the Thermal Activation and Reconstruction of Hydrotalcite-like Compounds. *J. Phys. Chem. C* **2007**, *111* (9), 3642–3650.
- (53) Bedolla-Valdez, Z. I.; Ramirez-Solis, S.; Prince, J.; Lima, E.; Pfeiffer, H.; Valente, J. S. Dynamic water vapor sorption on $\text{Mg}(\text{Ga}^{3+})\text{O}$ mixed oxides: Analysis of the LDH thermal regeneration process. *Thermochim. Acta* **2013**, *553*, 49–53.
- (54) Pérez-Ramírez, J.; Abello, S.; van der Pers, N. M. Memory effect of activated Mg–Al hydrotalcite: in situ XRD studies during decomposition and gas-phase reconstruction. *Chem. - Eur. J.* **2007**, *13* (3), 870–878, DOI: 10.1002/chem.200600767.
- (55) Buffet, J.-C.; Byles, C. F.; Felton, R.; Chen, C.; O'Hare, D. Metallocene supported core@LDH catalysts for slurry phase ethylene polymerisation. *Chem. Commun.* **2016**, *52* (21), 4076–4079.
- (56) Kenyon, P.; Leung, D. W. J.; Lyu, M.; Chen, C.; Turner, Z. R.; Buffet, J.-C.; O'Hare, D. Controlling the activity of an immobilised molecular catalyst by Lewis acidity tuning of the support. *J. Catal.* **2021**, *402*, 94–100.
- (57) Kenyon, P.; Leung, D. W. J.; Turner, Z. R.; Buffet, J.-C.; O'Hare, D. Tuning Polyethylene Molecular Weight Distributions Using Catalyst Support Composition. *Macromolecules* **2022**, *55* (9), 3408–3414.
- (58) Kaneyoshi, M.; Jones, W. Formation of Mg–Al layered double hydroxides intercalated with nitrilotriacetate anions. *J. Mater. Chem.* **1999**, *9* (3), 805–811.
- (59) Kukkadapu, R. K.; Witkowski, M. S.; Amonette, J. E. Synthesis of a Low-Carbonate High-Charge Hydrotalcite-like Compound at Ambient Pressure and Atmosphere. *Chem. Mater.* **1997**, *9* (2), 417–419.
- (60) Greenwell, H. C.; Jones, W.; Stamires, D. N.; O'Connor, P.; Brady, M. F. A one-pot synthesis of hybrid organo-layered double hydroxide catalyst precursors. *Green Chem.* **2006**, *8* (12), 1067–1072, DOI: 10.1039/b605851e.
- (61) Pushparaj, S. S. C.; Forano, C.; Prevot, V.; Lipton, A. S.; Rees, G. J.; Hanna, J. V.; Nielsen, U. G. How the Method of Synthesis Governs the Local and Global Structure of Zinc Aluminum Layered Double Hydroxides. *J. Phys. Chem. C* **2015**, *119* (49), 27695–27707.
- (62) Pimentel, C.; de la Luz, A. P.; Hernández-Laguna, A.; Sainz-Díaz, C. I. Effects of the cation ordering in Mg:Al and Zn:Al layered double hydroxides on crystallographic and spectroscopic properties by means of first principles calculations. *Appl. Clay Sci.* **2022**, *223*, No. 106496, DOI: 10.1016/j.clay.2022.106496.
- (63) Sideris, P. J.; Nielsen, U. G.; Gan, Z.; Grey, C. P. Mg/Al ordering in layered double hydroxides revealed by multinuclear NMR spectroscopy. *Science* **2008**, *321* (5885), 113–117.
- (64) Cadars, S.; Layrac, G.; Gérardin, C.; Deschamps, M.; Yates, J. R.; Tichit, D.; Massiot, D. Identification and Quantification of Defects in the Cation Ordering in Mg/Al Layered Double Hydroxides. *Chem. Mater.* **2011**, *23* (11), 2821–2831.
- (65) Sideris, P. J.; Blanc, F.; Gan, Z.; Grey, C. P. Identification of Cation Clustering in Mg–Al Layered Double Hydroxides Using Multinuclear Solid State Nuclear Magnetic Resonance Spectroscopy. *Chem. Mater.* **2012**, *24* (13), 2449–2461.
- (66) Zhao, L.; Qi, Z.; Blanc, F.; Yu, G.; Wang, M.; Xue, N.; Ke, X.; Guo, X.; Ding, W.; Grey, C. P.; Peng, L. Investigating Local Structure in Layered Double Hydroxides with ^{17}O NMR Spectroscopy. *Adv. Funct. Mater.* **2014**, *24* (12), 1696–1702.
- (67) Leonardelli, S.; Facchini, L.; Fretigny, C.; Tougne, P.; Legrand, A. P. Silicon-29 NMR study of silica. *J. Am. Chem. Soc.* **1992**, *114* (16), 6412–6418.
- (68) d'Espinose de la Caillerie, J.-B.; Kermarec, M.; Clause, O. ^{29}Si NMR Observation of an Amorphous Magnesium Silicate Formed during Impregnation of Silica with Mg(II) in Aqueous Solution. *J. Phys. Chem. A* **1995**, *99* (47), 17273–17281.
- (69) Brew, D. R. M.; Glasser, F. P. Synthesis and characterisation of magnesium silicate hydrate gels. *Cem. Concr. Res.* **2005**, *35* (1), 85–98.
- (70) Valla, M.; Rossini, A. J.; Caillot, M.; Chizallet, C.; Raybaud, P.; Digne, M.; Chaumonnot, A.; Lesage, A.; Emsley, L.; van Bokhoven, J. A.; Copéret, C. Atomic Description of the Interface between Silica and Alumina in Aluminosilicates through Dynamic Nuclear Polarization Surface-Enhanced NMR Spectroscopy and First-Principles Calculations. *J. Am. Chem. Soc.* **2015**, *137* (33), 10710–10719.
- (71) Lippmaa, E.; Maegi, M.; Samoson, A.; Tarmak, M.; Engelhardt, G. Investigation of the structure of zeolites by solid-state high-resolution silicon-29 NMR spectroscopy. *J. Am. Chem. Soc.* **1981**, *103* (17), 4992–4996.
- (72) Man, P. P.; Peltre, M. J.; Barthomeuf, D. Nuclear magnetic resonance study of the dealumination of an amorphous silica–alumina catalyst. *J. Chem. Soc., Faraday Trans.* **1990**, *86* (9), 1599–1602.
- (73) Bocclair, J. W.; Braterman, P. S. Layered double hydroxide stability. 1. Relative stabilities of layered double hydroxides and their simple counterparts. *Chem. Mater.* **1999**, *11* (2), 298–302.
- (74) Gao, Y.; Zhang, Z.; Wu, J.; Yi, X.; Zheng, A.; Umar, A.; O'Hare, D.; Wang, Q. Comprehensive investigation of CO_2 adsorption on Mg–Al– CO_3 LDH-derived mixed metal oxides. *J. Mater. Chem. A* **2013**, *1* (41), 12782–12790.
- (75) Kim, B.-K.; Gwak, G.-H.; Okada, T.; Oh, J.-M. Effect of particle size and local disorder on specific surface area of layered double hydroxides upon calcination-reconstruction. *J. Solid State Chem.* **2018**, *263*, 60–64.